

Article

Corrosion Study of Pipeline Steel under Stress at Different Cathodic Potentials by EIS

Ricardo Galván-Martínez ¹, Ricardo Orozco-Cruz ^{1,*}, Andrés Carmona-Hernández ¹,
Edgar Mejía-Sánchez ¹, Miguel A. Morales-Cabrera ² and Antonio Contreras ³

¹ CA-245- Ingeniería de Corrosión y Protección, Instituto de Ingeniería, Universidad Veracruzana, S. S. Juan Pablo II, Zona Universitaria, Boca del Río, Veracruz 94294, Mexico; rigalvan@uv.mx (R.G.-M.); andres_carmona_hernandez@hotmail.com (A.C.-H.); edmejia@uv.mx (E.M.-S.);

² Facultad de Ciencias Químicas, Universidad Veracruzana, Circuito Gonzalo Aguirre Beltrán S/N, Zona Universitaria, Xalapa, Veracruz 91000, Mexico; miguelmorales.uv@gmail.com

³ Instituto Mexicano del Petróleo, Eje Central Lázaro Cárdenas Norte 152, Col. San Bartolo Atepehuacan, Alcaldía Gustavo A. Madero, Ciudad de México 07730, Mexico; acontrer@imp.mx

* Correspondence: rorozco@uv.mx

Received: 13 November 2019; Accepted: 11 December 2019; Published: 16 December 2019

Abstract: The effect of different cathodic potentials applied to the X70 pipeline steel immersed in acidified and aerated synthetic soil solution under stress using a slow strain rate test (SSRT) and electrochemical impedance spectroscopy (EIS) was studied. According to SSRT results and the fracture surface analysis by scanning electron microscopy (SEM), the steel susceptibility to stress corrosion cracking (SCC) increased as the cathodic polarization increased (E_{cp}). This behavior is attributed to the anodic dissolution at the tip of the crack and the increment of the cathodic reaction (hydrogen evolution) producing hydrogen embrittlement. Nevertheless, when the E_{cp} was subjected to the maximum cathodic potential applied (-970 mV), the susceptibility decreased; this behavior is attributed to the fact that the anodic dissolution was suppressed and the process of the SCC was dominated only by hydrogen embrittlement (HE). The EIS results showed that the cathodic process was influenced by the mass transport (hydrogen diffusion) due to the steel undergoing so many changes in the metallic surface as a result of the applied strain that it generated active sites at the surface.

Keywords: X70 steel; stress corrosion cracking (SCC); slow strain rate tests (SSRT); electrochemical impedance spectroscopy (EIS); cathodic potentials

1. Introduction

Stress corrosion cracking (SCC) is one of the most important causes of failures in buried pipelines, mainly in the transport of hydrocarbons [1,2]. The environments that generate SCC in the pipelines are generally electrolytes caught between the detached coating and the surface of the pipeline steel. According the characteristics of electrolytes developed under disbonded coatings, pipelines can suffer two different types of SCC: high-pH SCC, and near-neutral pH SCC [3,4]. The SCC at high pH generally occurs as a result of the generation of a concentrated solution of carbonate-bicarbonate ($\text{pH} > 9$) with an intergranular crack morphology. This mechanism is attributed to selective anodic dissolution of the grain border and to the repeated rupture of the passive film that forms in the tip of the crack. On the other hand, the SCC at almost neutral pH (pH 5–8.5) is associated with diluted solutions generated by the underground water with a transgranular crack morphology; [5–7] however, there is no consensus about its mechanism. Some research [8–10] proposes that the crack can be induced by the synergic effect between the anodic dissolution and the

diffusion of the H in the steel. In addition, some SCC types have been found in acid environments (pH 3–6), where the surface of the pipeline is in direct contact with the soil in coating defects [11]. Nevertheless, the SCC behavior in acid soils is not clear, and investigations into it have not been well defined [3].

Cathodic protection (CP) is one of the most important methods of protection against the corrosion in buried pipelines; however, this CP can contribute to the SCC process through hydrogen generation. The current in the CP can fluctuate as a result of the permeability of the coating and variations in soil resistivity, provoking potential fluctuations in some zones of the pipeline steel and generating the formation of localized corrosion, such as pitting and crevice corrosion. Pitting corrosion in combination with the stress (residual or operational) in the pipeline can nucleate and generate cracks [12].

Some researchers [13–16] have studied the influence of CP in the SCC susceptibility of steels, and determined that CP could influence in the mechanism of cracking induced by SCC. Liu et al. [16] investigated the SCC mechanism of X70 steel under different cathodic potentials (E_{cp}) in a synthetic soil solution with an almost neutral pH; they found a critical potential interval (from -730 to -920 mV vs. saturated calomel electrode); if the E_{cp} was more positive than above interval, the SCC mechanism would be based on the anodic dissolution of the steel, but if the E_{cp} were more negative, the SCC mechanism would be hydrogen embrittlement. Finally, if the E_{cp} had a value in between, the SCC would present both mechanisms.

In this work, electrochemical polarization measurements were combined with slow strain rate tensile (SSRT) tests and surface characterization to investigate the relationship between the SCC characteristics and the electrochemical corrosion properties of an API X70 steel in a near-neutral pH solution.

This research was focused on characterizing the SCC process of X70 pipeline steel immersed in synthetic soil solution under the application of different cathodic potentials, using a slow strain rate test (SSRT) and electrochemical impedance spectroscopy (EIS).

2. Materials and Methods

2.1. Working Electrode

The material used in the present study as working electrode was API 5L X70 pipeline steel with a chemical composition as shown in Table 1. Steel samples were obtained from a pipeline that had an external diameter of 36 in (914.4 mm) and a wall thickness of 0.902 in. (22.91 mm). The samples used in the slow strain rate test were machined according to NACE TM 0198 [17].

The surface of the gauge section was polished up to 1200 SiC grit paper in an orientation parallel to the subsequent loading direction of the SSRT in order to ensure similar surface conditions for all tests.

Table 1. Chemical composition of X70 pipeline steel (wt.%).

C	Mn	Si	P	S	Al	Nb	Cu	Cr	Ni	V	Ti	Fe
0.031	1.48	0.13	0.012	0.002	0.033	0.1	0.29	0.27	0.16	0.004	0.012	Balanced

2.2. Test Solution

The corrosive environment used in all of the electrochemical tests was a simulated groundwater solution (called NS4) with a pH of 3. NS4 synthetic solution has been used widely to simulate soil solution in the study of near neutral pH-SCC behavior. However, other synthetic soil solutions such as NS1, NS2, NS3, NS4 and NOVA have been used in similar studies. Table 2 shows the chemical composition of the NS4 solution used. The pH of the NS4 solution was around 8.0; however, for this study, the pH solution was adjusted with hydrochloric acid to obtain a pH of 3.

Table 2. Chemical composition of NS4 solution (g/L).

NaHCO ₃	CaCl ₂ ·2H ₂ O	MgSO ₄ ·7H ₂ O	KCl
0.483	0.181	0.131	0.122

2.3. Slow Strain Rate Tests (SSRT)

SSRT were carried out on smooth cylindrical tensile samples, using an MCERT machine (Mobile Constant Extension Rate Tests) at a strain rate of $1 \times 10^{-6} \text{ s}^{-1}$ in air and synthetic soil solution (NS4 solution). All SSRT were conducted at room temperature and atmospheric pressure. The length direction of the sample was parallel to the circumferential direction of the pipeline steel, with the goal that, if a crack appeared, it would grow in the longitudinal direction of the pipeline as is typically observed in underground pipelines. Cylindrical samples with a reduced length of 1 inch and 0.150 inches in diameter were machined with a total exposed area of 3.04 cm². These cylindrical samples were machined according to the NACE TM 0198 standard [17]. After the SSRT was completed, the fractured sample was removed, and cleaned using inhibited acid and acetone for SEM examination.

2.4. Electrochemical Impedance Spectroscopy (EIS)

The EIS measurements were carried out simultaneously with the SSRT using a potentiostat/galvanostat and an electrochemical cell with a three-electrode arrangement where the working electrode was the X70 pipeline steel, sintered graphite bar was used as the auxiliary electrode, and saturated calomel electrode, SCE, was used as the reference electrode. In all EIS tests, the frequency range from 0.01 to 10 kHz with the amplitude of 0.01 V against to E_{corr} was used. Seven points per decade of frequency were recorded. In order to apply the overvoltage to the working electrode, an external direct current source and a second auxiliary electrode were used to close the circuit in the cathodic protection system by impressed current.

EIS tests and SSRT were carried out at corrosion potential ($E_{\text{corr}} = -650 \text{ mV vs. SCE}$) and at three different cathodic potentials (E_{cp}): -770 mV (cathodic protection potential, CPP), -870 mV (100 mV of overvoltage as a function of CPP), and -970 mV (200 mV of overvoltage as a function of CPP) and compared to the saturated calomel electrode.

2.5. Potentiodynamic Polarization Curves (PC)

Two polarization curves were recorded at two different sweep rates, at 5 mV and 50 mV per second. All PC were carried out at room temperature atmospheric pressure and without stress conditions. The focus of this experiment is to predict a potential range where the steel is susceptible to SCC. Polarization range used in the carry out the PC was from -1400 mV to 0 vs. SCE.

3. Results and Discussion

3.1. SSRT at Different Cathodic Potentials (E_{cp})

Figure 1 shows the stress (σ) vs. strain (ϵ) curve of X70 pipeline steel immersed in acidified NS4 solution (pH 3) at the E_{corr} (-650 mV vs. SCE) and at different applied cathodic potentials (-770 , -870 and -970 mV vs. SCE) during the SSRT.

According to Figure 1, the profiles at the different cathodic potentials show an increase in the yielding strength (σ_{YS}) and ultimate tensile strength (σ_{UTS}) compared to the test in air. This increment is attributed to the diffusion of atomic hydrogen (H) into the crystal lattice, because the E_{cp} thermodynamically favors the evolution reaction of the H [18]. According to Liu et al. [16], there is a critical concentration of H ($C_{\text{H,crit}}$) that determines the increase or decrease of σ_{YS} . When the H concentration (C_{H}) on metallic surface is below the $C_{\text{H,crit}}$, the H impedes the sliding dislocations that generate the increment of the σ_{YS} . However, if the C_{H} exceeds the $C_{\text{H,crit}}$ value, the dislocations activity is facilitated, and the σ_{YS} decreases.

In accordance with this fact, the σ_{YS} increased between the E_{corr} and -870 mV vs. SCE, because the C_H also increased. It is important to point out that the C_H did not exceed the $C_{H,crit}$. At -970 mV vs. SCE, the σ_{YS} decreased because the C_H exceeded the $C_{H,crit}$.

The SCC susceptibility of X70 steel was calculated on the basis of the reduction area percent (%RA) and the plastic elongation (%PE), using the following equations:

$$\%RA = \frac{D_i^2 - D_f^2}{D_i^2} \times 100, \quad (1)$$

where D_i and D_f are the initial and final diameter of the fracture surface.

$$\%PE = \left\{ \frac{E_f}{L_i} - \left[\frac{\sigma_F}{\sigma_{PL}} \right] \times \frac{E_{PL}}{L_i} \right\} \times 100, \quad (2)$$

where E_f is the elongation at failure, L_i the initial gauge length, σ_F is the stress at failure; σ_{PL} is the stress at the proportional limit, E_{PL} is the elongation at the proportional limit.

The SCC index considering %RA and %PE were calculated according to the following equations:

$$I_{RA} = RA_{sol} / RA_{Air}, \quad (3)$$

$$I_{PE} = PE_{sol} / PE_{Air}, \quad (4)$$

where the suffix Sol and Air correspond to the values obtained in the NS4 solution and air, respectively. The I_{RA} and I_{PE} are the SCC susceptibility indexes.

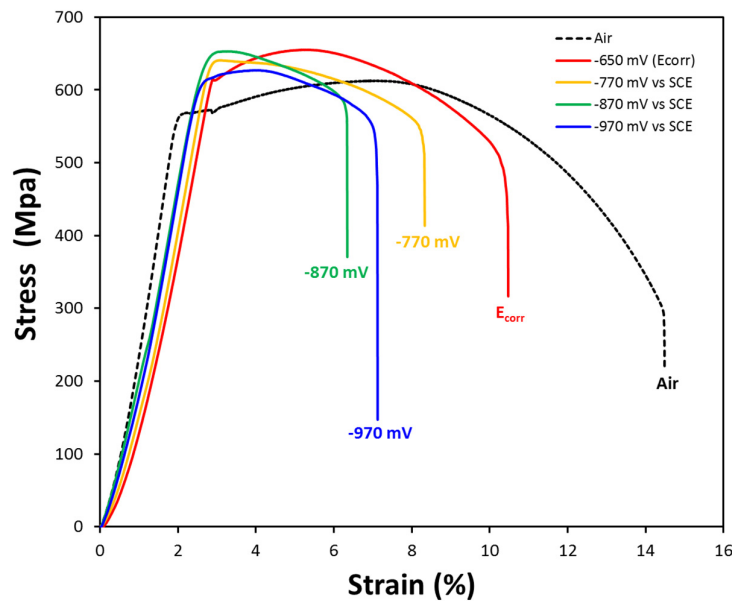


Figure 1. Stress-strain (σ vs. ϵ) curves of X70 pipeline steel immersed in NS4 solution (pH 3) at the E_{corr} (-650 mV vs. SCE) under the application of different cathodic potentials.

According to the indexes (I_{RA} and I_{PE}) shown in Figure 2, and to the classification proposed by McIntyre et al. [19], the X70 steel at E_{corr} had moderate susceptibility to SCC, but when the X70 steel was analyzed with different E_{cp} , the steel exhibited great susceptibility to SCC.

The I_{RA} and I_{PE} values decreased as the E_{cp} became more negative; however at the E_{cp} of -970 mV vs. SCE, the indexes increased, indicating a slight decrease in the susceptibility to SCC. The SCC susceptibility of X70 steel shows a complex dependence on cathodic potential.

As it is showed in the Figure 2, the SCC susceptibility tends to increase as the potential reaches more negative values. With the different applied cathodic potentials, the SCC process changes. At less negative potential (-650 and -770 mV), the SCC is based primarily on the anodic dissolution mechanism. When the applied potential reaches more negative values, hydrogen is involved in the

cracking process (-870 and -970 mV), resulting in a transgranular cracking mode with brittle feature of the fracture surface.

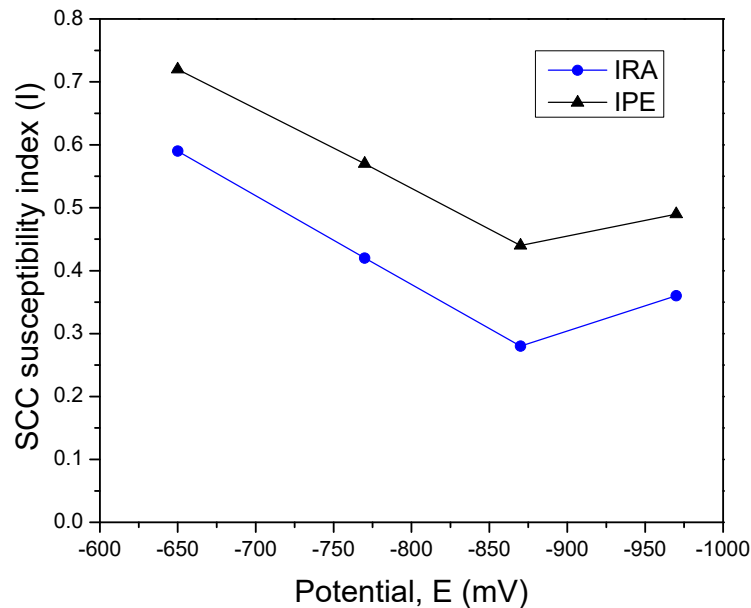


Figure 2. SCC susceptibility indexes of X70 pipeline steel as a function of potential.

Generally, more negative cathodic potentials enhance the hydrogen evolution reaction. Therefore, it is commonly assumed that there will be more hydrogen atoms penetrating into the steel, contributing to the SCC process. According to the Pourbaix diagram, it can be observed that over potential applied to steel specimens (-870 and -970 mV) results in hydrogen evolution. The concentration of hydrogen atoms depends on cathodic potential; as cathodic potential decreases, a greater concentration of hydrogen atoms is generated. Hydrogen can diffuse into the steel specimen around the crack tip during the SCC process, resulting in hydrogen embrittlement, leading to increased SCC susceptibility. Cheng [8] developed a thermodynamic model to illustrate the interaction of hydrogen, stress and anodic dissolution at the crack tip. He suggested that crack growth rate was dependent on the synergistic effect of hydrogen and stress, and the concentration of hydrogen atoms.

3.2. Surface Fracture after SSRT

Figure 3 shows SEM micrographs of the fractured surface of X70 pipeline steel at two different magnifications (100X and 1000X) after performing SSRT in air and NS4 solution (pH 3) at the E_{corr} (-650 mV) and when different cathodic potentials (-770 , -870 and -970 mV vs. SCE) were applied.

The X70 steel tested in air exhibited a ductile fracture type, Figures (3a, a1). The same behavior was observed for samples tested at -650 , Figures (3b, b1) and -770 mV, Figures (3c, c1). In these figures, the dimples produced by micro-plastic deformation can be observed, as well as the presence of micro-pores that can act as stress concentrators, with these sites being the typical places where cracking is preferentially generated. These micropores produce metal cracking by the coalescence mechanism [13,20].

Figures 3(d, d1) and 3(e, e1) shows the fracture surface for samples tested at -870 and -970 mV, respectively. In these figures, a mix fracture types—ductile and brittle—can be observed. The presence of some brittle regions and the presence of some microcracks can be clearly observed. Most of the samples with cathodic potentials of -870 and -970 mV show the presence of some internal cracks, which is correlated with the more brittle fracture type observed in these samples.

It is important to point out that Lynch et al. [21] found that the hydrogen embrittlement induced by the medium could produce ductile fracture through the Adsorption Induced Dislocation

Emission (AIDE) mechanism. The AIDE mechanism includes both nucleation and subsequent movement of dislocations away from the crack tip. This mechanism consists of the weakening of the interatomic bond at the tip of the crack due to adsorbed hydrogen; this behavior promotes a change in the fracture to a relatively lower deformation due to the local reduction of ductility.

In Figures 3(d, d1) and 3(e, e1), it is possible to observe internal cracks, which can be indicative of the diffusion of hydrogen into the steel; the hydrogen is preferentially trapped in some defects such as microcavities and inclusions, the crystalline lattice is dilated, and the interatomic cohesion decreases, leading to the appearance of internal cracks. It is generally known that pitting and pre-existing defects initiate SCC; the lattice defects—vacancies, dislocations, grain boundaries and precipitates—provide a variety of trapping sites for hydrogen diffusion. Hydrogen diffusion promotes both intergranular and transgranular cracking.

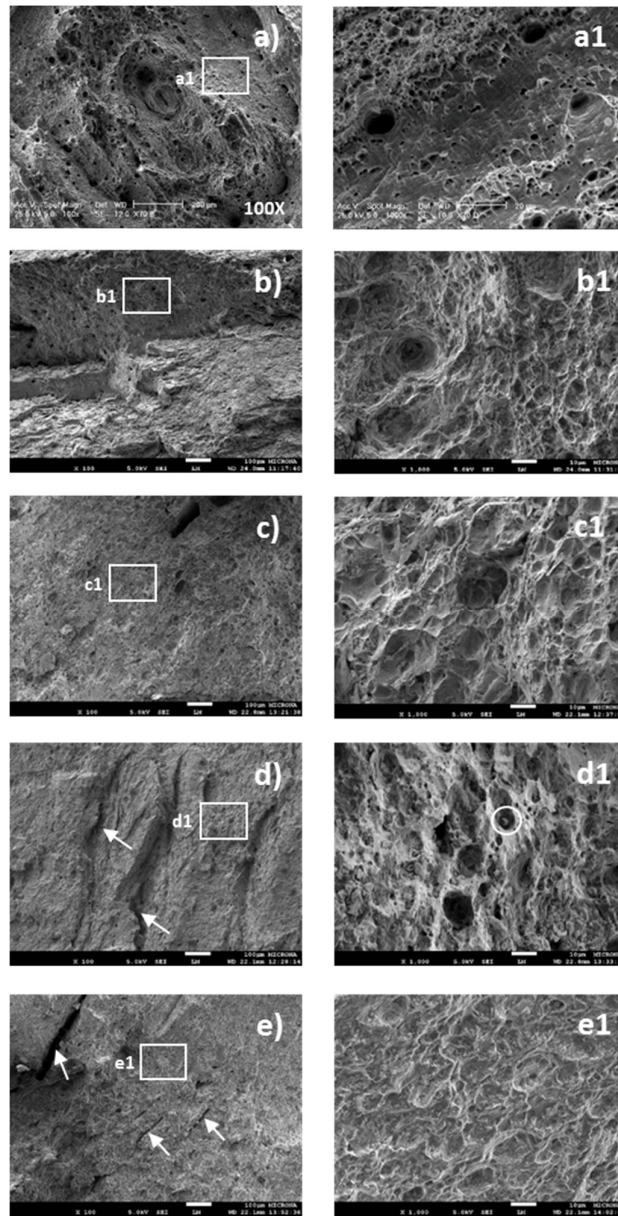


Figure 3. SEM micrographs of the fracture surface of X70 steel after performing SSRT at two different magnifications (100X and 1000X): (a, a1) in air; and (b, b1) in NS4 solution with $E_{corr} = -650$ mV, and in NS4 solution with different cathodic potentials, (c, c1) -770 mV, (d, d1) -870 mV, and (e, e1) -970 mV.

The hydrogen atoms diffuse into the metal and have a preference for accumulating in internal defects like inclusions, precipitates, cavities, and dislocations, among others. Hydrogen atoms in these regions result in embrittlement, and when the stress increases to a critical value, cracking is initiated. It is important to note that the level of stress or strain depends on the steel grade. High tensile strength steels with elasticity limits exceeding 650 MPa are highly susceptible to SCC. Martensitic structures are considerably more susceptible than bainitic and ferrite structures. In addition, coarse-grained materials are more susceptible to embrittlement than fine microstructures.

Crack propagation can be either intergranular or transgranular; sometimes, both types are observed on the same fracture surface. In the case of near neutral pH-SCC at corrosion potential (-680 to -710 mV SCE), a transgranular crack morphology is generally observed. Meanwhile, with high pH SCC, intergranular cracking is commonly observed in the potential range of -520 to -670 mV SCE.

It is important to point out that in Figures 3(d, d1) (-870 mV), it is possible to observe some inclusions that could have contributed to the cracking. Liu et al. [22] concluded that the inclusions in the X70 steel are rich in brittle oxides that are incoherent with the matrix of the steel; thus, a great deformation of the crystalline lattice is formed. This deformation is the main factor for the preferential generation of microcracks between the borders of these inclusions and the steel.

Finally, at -970 mV, Figures 3(e, e1) it is possible to observe that the fracture morphology is different from the morphologies found at -770 and -870 mV, because the surface of the fracture shows a smooth scission of brittle character, corresponding to the SCC process dominated by the hydrogen embrittlement. This fact indicates that the concentration of the atomic hydrogen adsorbed on the surface of the X70 steel was greater when the E_{cp} was applied, resulting in an increase in yield strength (YS) and ultimate tensile strength (UTS), but decreases in strain and elongation (Figure 1) due to the embrittlement of the microstructure. According to this behavior, it is possible to say that the mechanism in the SCC process was hydrogen-enhanced localized plasticity (HELP), which improves the movement of dislocations because they are surrounded by atomic hydrogens, facilitating plastic deformation in a localized way. According to Martin et al. [23], the hydrogen-enhanced localized plasticity (HELP) mechanism as a viable mechanism of hydrogen embrittlement.

Hydrogen embrittlement (HE) has been studied for many years; however, it remains a consistent problem in the SCC process. In addition, there is no precise mechanism for HE. Various mechanisms proposed in the literature include hydrogen-enhanced decohesion and hydrogen-enhanced local plasticity (HELP) [23].

The HELP mechanism is supported by experimental observations of enhanced dislocation motion and localized slip bands in the vicinity of the crack tip in hydrogen-charged test specimens. The most accepted mechanism for enhancing HELP is that hydrogen increases dislocation mobility, leading to the material being more ductile.

3.3. Cracks in the Gauge Section after SSRT

The secondary cracking commonly presented in the gauge section of the specimen corresponded to typical cracking in a medium that promotes the SCC process. Figure 4 shows some images obtained by SEM of cracks located in the gauge section of the SSR specimens. These cracks were sharp and without ramifications, which is characteristic of a hydrogen-induced cracking (HIC) process [3]. On the other hand, the cracks observed in the steel at the E_{corr} (Figure 4a) show ramifications and aggressive attacks on the surface with no cracks, produced by the anodic activity that prevails under these conditions.

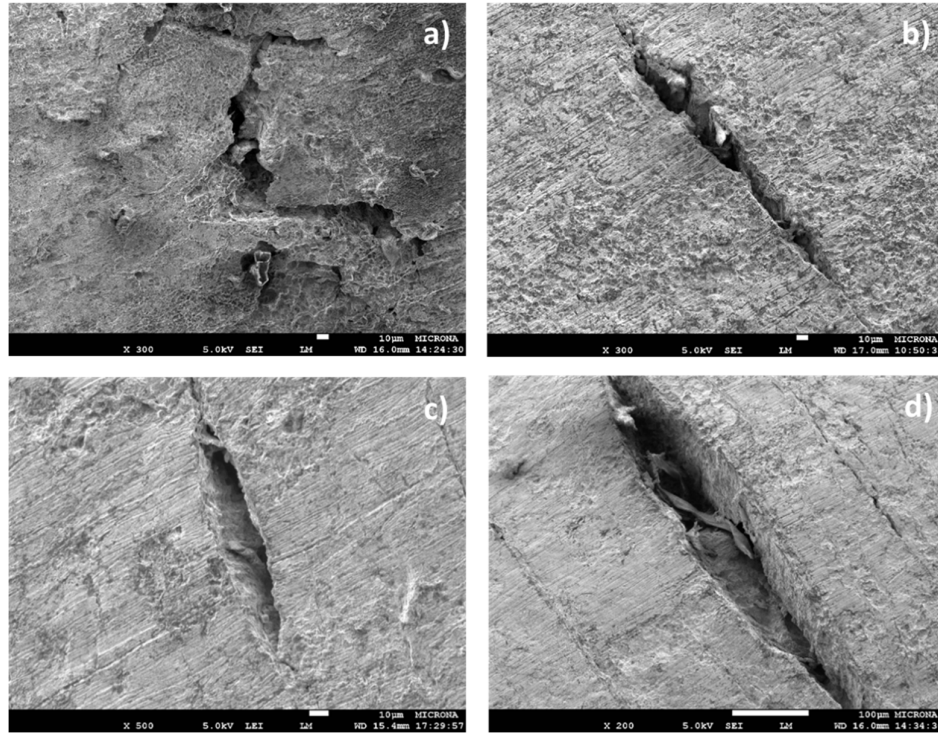


Figure 4. Secondary cracking of X70 pipeline steel after SSRT: (a) -650 mV (E_{corr}), (b) -770 mV (c) -870 mV (d) -970 mV vs. SCE.

3.4. SCC Analysis under different E_{cp} by Polarization Curves

To gain a better understanding of the SCC mechanism of X70 steel under different cathodic potentials, a conceptual model developed by Liu et al. [16] was used. This model is based on the polarization curves (PC) of the X70 steel without stress at fast and slow sweep rates. Figure 5 shows three zones or potential intervals between the two polarization curves (at fast and slow sweep rate) of the X70 steel immersed in the NS4 solution (pH 3), limited by the potential values where the current density trends to zero. Zone I corresponds to potential values lower than -700 mV vs. SCE, where the PCs at both sweep rates are located in the anodic polarization region. Zone II is localized to the interval between -700 and -900 mV vs. SCE. In this zone, the PC obtained with the slow sweep rate was found to be in the cathodic polarization region, while the PC obtained with the fast sweep rate was found to be in the anodic polarization region; finally, zone III encompasses the more negative potential at -970 mV vs. SCE, where the two PCs, at both sweep rates, were located in the cathodic polarization region [24]. According to the behavior of the three zones, if the X70 steel is polarized with a potential that is in zone I, this fact indicates that in the tip of the crack, in the wall of the crack and in the uncracked metallic surface, the anodic reaction mainly could be carried out, and the cracking mechanism would depend only on the anodic dissolution. If the applied potential is found in zone II, this fact indicates that the anodic dissolution can be carried out in the tip of the crack, contributing to the acceleration of its propagation, while in the uncracked metallic surface, hydrogen reduction is carried out on other species like O_2 and H_2CO_3 ; therefore, the SCC process can be controlled by the combination of two processes, the mechanism of the hydrogen embrittlement and the anodic dissolution.

On the other hand, if the applied potential is found in zone III, it means that in the tip and wall of the crack could benefit the cathodic reaction, specifically the H reduction, generating H atoms with this reaction that can then be actively involved in the SCC process. These results are in agreement with the research of Javidi and Galvan-Martinez [24,25]. Accordingly, the SCC mechanism would be dominated by hydrogen embrittlement.

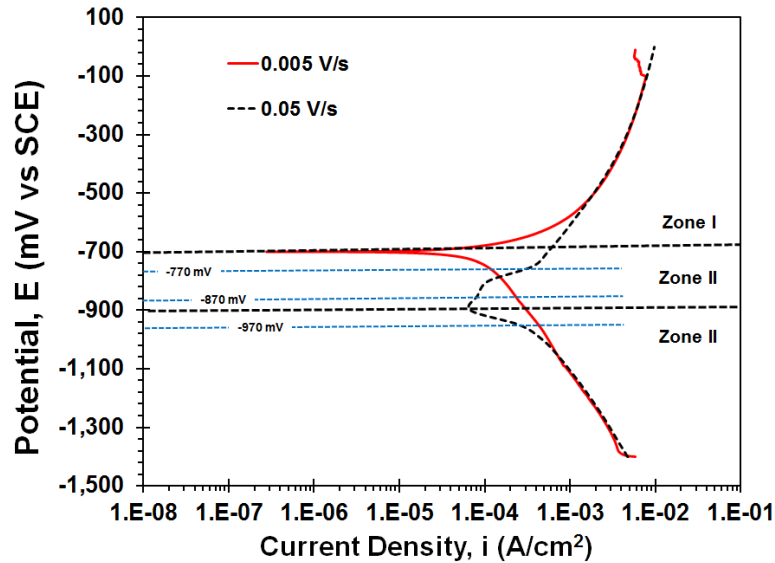


Figure 5. Polarization curves of the X70 steel in NS4 solution at two different sweep rates: 5 mV/s and 50 mV/s.

In addition, in Figure 5, it is possible to observe that the E_{cp} of -0.77 and -0.87 V vs. SCE are within zone II, while the E_{cp} of -0.97 V vs. SCE is located in zone III. Therefore, the behavior of the SCC susceptibility with respect to E_{cp} , as shown in Figure 2, can be attributed to the contribution of the anodic dissolution on the SCC mechanism. That is, when the potential is sufficiently negative, the anodic dissolution of the steel will be negligible and will not contribute to the SCC process, and this process will be dominated only by hydrogen embrittlement; on the other hand, at more positive potentials, even when the steel is under cathodic protection, in the area of tip of the crack, the steel will be in a non-stationary state and the anodic dissolution will contribute to the cracking process.

3.5. Qualitative analysis of the EIS Spectra

EIS measurements of the X70 pipeline steel immersed in NS4 solution (pH 3) at the E_{corr} and at under different E_{cp} (-0.77 , -0.87 and -0.97 V vs. SCE) are shown in Figure 6. It is important to point out that five different points were measured in the stress strain curve at each E_{cp} : at beginning of the test (T0), in the elastic zone (EZ), at yield strength (YS), at ultimate tensile strength (UTS), and before fracture (BF). In Figure 6, the experimental data (dots) and the fit line (continuous line) can be observed.

The EIS spectra of the X70 steel at the five points recorded and at the E_{corr} (Figure 6a) show a characteristic semicircle of a capacitive process related to the electrochemical double layer capacitance (C_{dl}) and the charge transfer resistance (R_{ct}) associated with the redox reactions that occur at the electrolyte/metal interface. On the basis of this behavior, the proposal for fitting the EIS spectra is a simple equivalent electric circuit (EEC) including only the charge transfer resistance process, the most common of which is the Randles circuit. It is important to point out that all EIS spectra only show one time constant, which is attributed to the activation process or, as it is also called, charge transfer resistance.

In addition, the R_{ct} decreased from T0 to UTS, and increased again at the BF point. The decrease of the R_{ct} should be attributed to the gradual increase of the stress that prompting the generation and concentration of dislocations in the metal and the formation of active sites close to tip of the crack [23,26], and to the hydrogen (H) diffusion into the metal, whereby H comes from the cathodic reaction. Cheng [8] proposed that the combination of the H and stress causes the anodic dissolution to be more thermodynamically favorable. Finally, the increase of the R_{ct} at the BF point is attributed to effects of corrosion film products on the cracked surface.

At E_{cp} of -0.77 and -0.87 V vs. SCE (Figure 6b,c) and at the T0 point, the EIS spectrum shows a capacitive semicircle that can be attributed to the charge transfer process. However, at the EZ, YS, UTS and BF points, it is possible to observe two time constants (τ): the first τ , located between the high and middle frequencies, is attributed to the charge transfer process; while the second τ is attributed to the mass transfer process. Some researchers, like Liu [24,27], have reported Nyquist plots with this behavior. Taking into consideration the fact that the SCC is a dynamic process (this is because in the Slow Strain Rate Tests the machine that carries out the extension of the metal sample applies a constant rate, $1 \times 10^{-6} \text{ s}^{-1}$) and the metallic surface during the SSRT can undergo small changes that affect the kinetics of the electrochemical reactions such that the transition from the activation to the mixing process is observed in the Nyquist plots of the EIS measurements between T0 and EZ. This behavior can be attributed to the model of local additional potential (LAP) proposed by Liu et al. [25,28]. When the steel subjected to stress is in the macroscopic elastic zone, the local concentration of the stress can result in defects such as microcracks and inclusions, which can generate active sites through the movement of the dislocations. Due to the steel being under cathodic polarization and the supplied flow of electrons being preferentially concentrated in these sites, a negative LAP is generated, which can benefit the cathodic process, and which can be diffused by the electroactive species because its consumption is faster than the supply at the interface. The mass transport from the bulk to the interface can thus be the limiting factor of the corrosion kinetics, specifically the cathodic process.

Finally, at 0.97 V vs. SCE, Figure 6d shows two τ when the steel was subjected to elastic stress (points T0 to LE). The τ corresponded to two overlapping capacitive semicircles. The τ was located in interval between high and medium frequencies was attributed to the charge transfer (activation process) from the interfaces to the metallic surface. Meanwhile, the τ located at low frequencies was attributed to the response of the adsorbed species, like hydrogen atoms and bubbles of molecular H_2 , on the surface, because when the voltage was applied to the steel, the hydrogen evolution (hydrogen reduction) increased, strongly provoking another interface with these hydrogens and generating a pseudo-capacitance phenomenon by adsorption. [26,29].

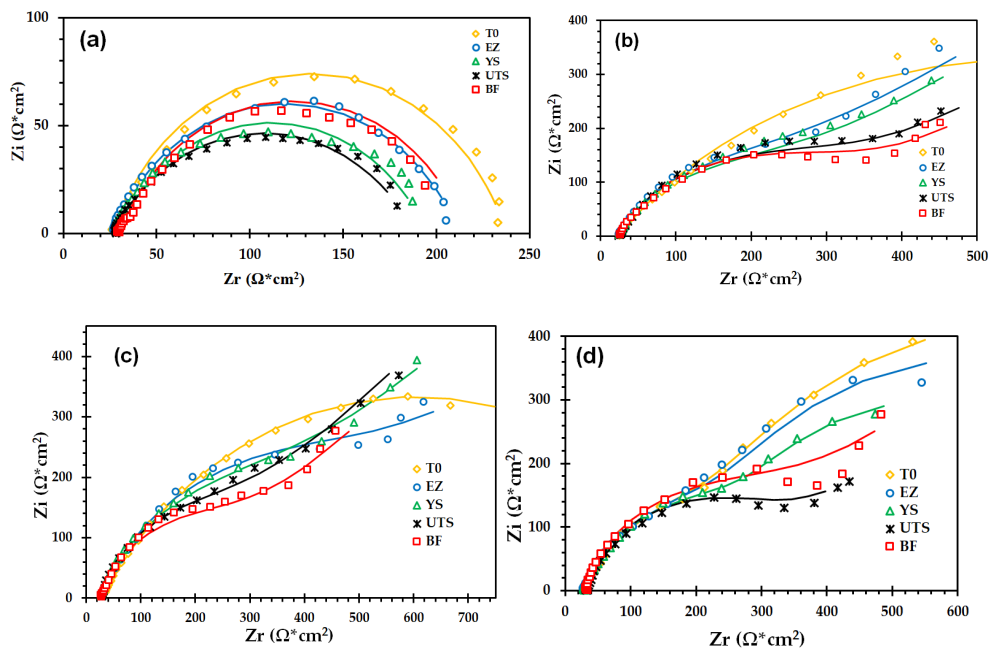


Figure 6. EIS spectra in Nyquist diagram of the X70 steel immersed in NS4 solution (with pH 3) during the SSRT test. At the E_{corr} (a), 0.77 (b), 0.87 (c) and 0.97 (d) V vs. SCE at different times. Dots correspond to experimental data and continuous lines correspond to fitting.

Pseudo-capacitance is the differential capacitance of an interface between the metal and the electrolyte, which is caused by the concentrated change of an adsorbed electroactive species and which is shown in electrochemical reactions where the charge transfer process precedes the determinant stage of the speed. It is important to point out that the electrolytic reaction of the hydrogen evolution (cathodic reaction) is an example of these electrochemical reactions. This is because in the first stage, the speed of the charge transfer could be fast, while in the second stage, the reaction between the two H atoms in order to form a H₂ molecule could be slow [27,30]. At the UTS and BF points, and in the low frequency zone, the τ changed to a straight line, which was attributed to the diffusion process.

3.6. Quantitative analysis of the EIS Spectra

Figure 7 shows the equivalent electric circuit (EEC) scheme and its physical explanation. According to Figure 7, it is possible to explain the EEC used in the fitting of the EIS spectra; that is to say, Figure 7a shows when the charge transfer process was the only process limiting the corrosion. As stated in the section 3.5, on Qualitative analysis, only one time constant can be observed in the EIS spectra, and this is attributed to the corrosion process. In the case of Figure 7b, the charge transfer process is influenced by a mass transfer of hydrogen ions or oxygen through the diffusion layer, in this case, the first time constant is attributed to the corrosion process and the second time constant to the diffusion process. Finally, Figure 7c shows the EEC with two time constants, but in this case the second constant is attributed to the layer of hydrogen reduced adsorbed on the metallic surface. It is important to point out that R_s is the solution resistance, and CPE_{dl} is the constant phase element of the double layer, which substitutes the double layer capacitor, because in real systems, the capacitive behavior of the electrode is not ideal. Due to corrosion products, film is adsorbed onto the metallic surface, and this generates a non-homogeneous surface. [28,31].

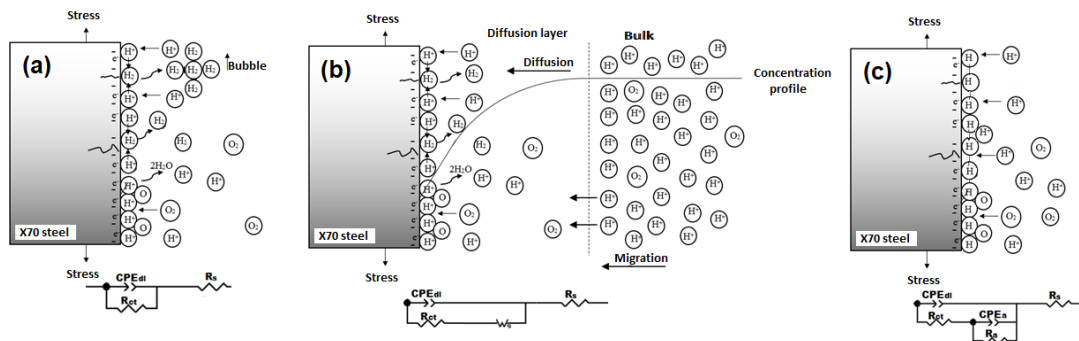


Figure 7. Scheme of EEC employed to fit the EIS spectra shown in Figure 6. (a) charge transfer process at T0, (b) diffusion process at EZ, YS, UTS and RS points, and (c) formation of a non-homogeneous surface at T0, EZ and YS points.

Figure 7 shows the EEC used to fit all of the EIS spectra in this research. All EIS spectra of the X70 steel obtained at the beginning of the test (T0) at E_{corr} and at different E_{cp} , -0.77 and -0.87 V vs. SCE, were fitted with a simple equivalent electric circuit (Figure 7a), the so-called Randles circuit.

Figure 7b shows the EEC used to fit the EIS spectra obtained at the EZ, YS, UTS and RS points. In this figure, (W_z) is the semi-infinite diffusion Warburg impedance (Z_w); in this case, the diffusion of the electroactive specie occurs when the mass transport is carried out from the bulk solution to the metallic surface in the absence of corrosion products [29,32]. When corrosion products are able to partially isolate the metallic surface, the study by Bastidas [33] defines the diffusion process for a layer of finite thickness using the transmission line model. Despite this model not being used in this research, it is important to note that this model is capable of providing a good analysis of corrosion. At E_{cp} of -0.97 V vs. SCE and at T0, EZ and YS, the EEC used is shown in Figure 7c [30]. In this EEC, it is possible to observe that an interface was adsorbed onto the metallic surface, and this can generate

an electric response [30,34]. The parameter R_a is the adsorbed resistance and CPE_a is the pseudo-capacitance associated with the adsorbed H. At the UTS and RS points, the EIS spectra were fitted with the Randles circuit.

To obtain a better analysis, the parameters calculated with the EEC fit of the EIS spectra shown in Figure 6 are presented in Table 3, where C_{dl} and C_a are the double layer and the adsorbed capacitance, respectively, calculated using the G. J. Brug expression [35]. It is important to point out that the CPE and R_{ct} values obtained in the EIS spectra fitting were used to calculate the capacitor by the Brug expression.

In this table, it is possible to see that the values of charge transfer resistance (R_{ct}), corresponding to the EIS spectra measured at the E_{corr} , have the lowest values. This fact indicates that the contribution of the anodic process tends to lead to a decrease in R_{ct} value and limits the SCC process. To obtain the influence of the E_{cp} on the corrosion phenomenon of X70 steel under stress conditions, an analysis with the R_{ct} as a function of the E_{cp} was carried out.

Table 3. Calculated parameters obtained for the EIS spectra of Figure 6 fitted by EEC in Figure 7.

Point	R_s		C_{dl}	R_{ct}		C_a	R_a		σ_w	
At the E_{corr} (−650 mV vs. SCE), Using the EEC Shown in Figure 5a										
	(Ωcm^2)	Error (%)	($\mu\text{F}/\text{cm}^2$)	(Ωcm^2)	Error (%)	($\mu\text{F}/\text{cm}^2$)	(Ωcm^2)	Error (%)	$\Omega\text{cm}^2 \text{ s}^{-0.5}$	Error (%)
T0	26.62	2.88	49.23	211	4.28	---	---	---	---	---
EZ	26.05	1.58	60.975	185.9	2.56	---	---	---	---	---
YS	27.24	1.73	62.22	168	3.01	---	---	---	---	---
UTS	26.43	1.63	72.45	162.1	3.08	---	---	---	---	---
BF	30.22	1.71	135.34	186	3.60	---	---	---	---	---
At −770 mV vs. SCE, using the EEC shown in Figure 5a (for T0) and Figure 5b										
T0	23.24	3.23	91.52	1135	14.20	---	---	---	--	---
EZ	24.09	2.99	75.73	305.82	7.26	---	---	---	278.90	11.93
YS	24.71	3.36	65.21	314.25	5.89	---	---	---	264.22	7.15
UTS	26.32	2.90	62.84	304.72	7.26	---	---	---	193.61	11.93
BF	26.00	2.56	57	295.41	4.55	---	---	---	179.64	5.49
At −870 mV vs. SCE, using the EEC show in Figure 5a (for T0) and Figure 5b										
T0	27.92	4.42	39.71	1056.00	11.20	---	---	---	--	---
EZ	28.11	3.43	55.19	496.04	8.31	---	---	---	203.99	4.70
YS	27.02	3.11	45.18	398.39	8.34	---	---	---	331.41	2.40
UTS	26.482	8.41	43.60	344.23	2.21	---	---	---	319.53	2.33
BF	27.505	10.86	50.15	268.13	2.10	---	---	---	241.60	3.53
At the E_{corr} (−970 mV vs. SCE) using the EEC show in Figure 5b (for UTS and BF) and Figure 5c										
T0	27.1	9.09	67.76	486.69	3.00	536.67	744.2	6.67	--	---
EZ	26.74	4.00	73.84	392.76	4.32	637.78	615.93	8.65	--	---
YS	28.04	7.06	83.04	332.79	2.15	625.46	642.78	7.10	--	---
UTS	36.08	4.46	104.99	302.02	2.66	--	--	---	110	3.76
BF	34.50	11.10	99.75	318.80	4.37	--	--	---	190.75	5.77

3.7. R_{ct} behavior as a function of E_{cp} .

Figure 8 shows the R_{ct} behavior obtained from the EEC shown in Figure 7. These R_{ct} were obtained from the corrosion phenomenon of the X70 steel immersed in NS4 solution at the E_{corr} and at different E_{cp} during the SSRT test. In a general way, it is possible to point out that at the E_{corr} , all R_{ct} values are lower than the R_{ct} values obtained at any E_{cp} . According to the mix potential theory, at the E_{corr} , the R_{ct} is the equilibrium result of the anodic and cathodic reactions occurring at the interface.

Some researchers, like Liu et al., have indicated that the R_{ct} can be expressed as follows [31,36]:

$$\frac{1}{R_{ct}} = \frac{1-\theta_c}{R_{ct,a}} + \frac{\theta_c}{R_{ct,c}} \quad (5)$$

where $R_{ct,a}$ and $R_{ct,c}$ are the charge transfer resistance for the anodic and cathodic reactions, respectively, θ_c is the fraction of the active area, where the cathodic reaction is carried out. When an E_{cp} is applied to the X70 steel, the $R_{ct,a}$ and θ_c will increase and $R_{ct,c}$ will decrease, with the R_{ct} value contributing to the cathodic process to a great extent. Therefore, at the E_{corr} , the anodic process contributes to a reduction in the R_{ct} value.

On the other hand, at the E_{cp} of -770 and -870 mV vs. SCE, the R_{ct} decreased throughout the entire time that the test was carried out. This behavior can be attributed to the propagation of the SCC in the tip of the crack, generating a new active surface, which is subject to a non-stationary stage of polarization. Liu et al. [24,27] proposed that the tip of the crack resembled an active specimen recently exposed to electrochemical medium; for this reason, the anodic dissolution in the main crack increases, contributing to the R_{ct} reduction.

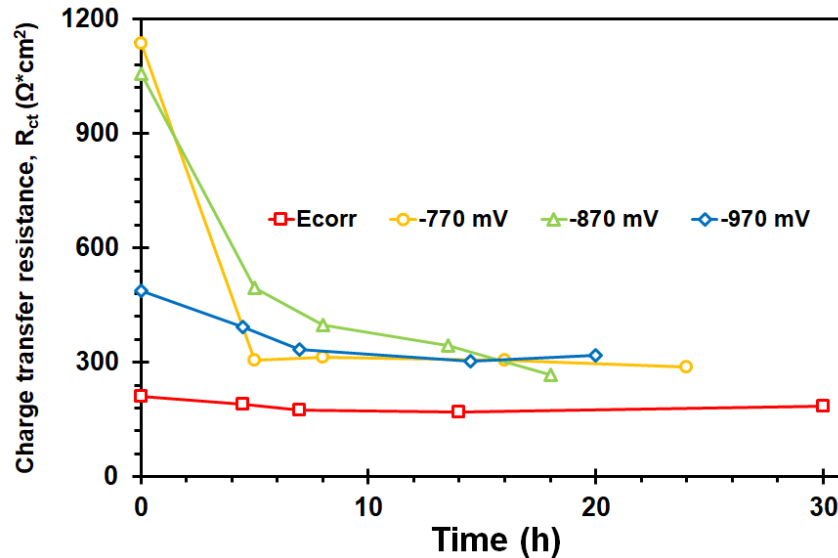


Figure 8. R_{ct} as a function of time. X70 steel immersed in NS4 solution (pH3) under different E_{cp} .

It is important to point out that at the beginning of the SSRT test, the R_{ct} was lower, as the E_{cp} was more negative due to the major supply of electrons to the interface, improving the cathodic reaction (Hydrogen evolution); however, when the stress levels increased, the R_{ct} became independent of the E_{cp} . This behavior can be attributed to the fact that as the SSRT test is carried out, the R_{ct} is a function of two parameters, the level stress and the applied potential, that can improve the cathodic process through the negative LAP generated at the active sites, and produced by the dislocation movement on the surface [25,28,31,34].

4. Conclusions

Characterization of the SCC process of X70 pipeline steel immersed in synthetic soil solution under the application of different cathodic potentials, using slow strain rate test (SSRT) and electrochemical impedance spectroscopy (EIS) allowed the following conclusions to be drawn:

- According to the SCC indexes obtained (I_{RA} and I_{PE}), it is clear that SCC susceptibility increases with the increase in cathodic potential. These indexes indicate that X70 steel could be susceptible to SCC.
- SEM observations revealed the presence of some internal cracks on the fracture surface (which is indicative of hydrogen diffusion); additionally, some secondary cracks in the gauge section of the SSRT specimens were observed. These cracks grew perpendicular to applied stress.
- The application of cathodic potentials (E_{cp}) decreased the corrosive attack on the metal surface; however, they increased the SCC susceptibility of the steel, which is attributed to the H^+ reduction process inducing hydrogen embrittlement by H diffusion into the steel.
- The influence of E_{cp} on the SCC susceptibility of X70 steel meant that by decreasing the E_{cp} from -770 to -870 mV, the SCC susceptibility increased through the improvement of the cathodic process and the contribution of the anodic dissolution at the tip of the crack. However, when the E_{cp} reached -970 mV, the susceptibility decreased, because the anodic dissolution of the steel

became negligible and the mechanism was dominated solely by hydrogen embrittlement. The above was verified with the analysis of the fracture surface using SEM.

- The results of EIS at -770 and -870 mV showed an active behavior at the beginning of the test, which changed to a mixed process when the steel was subjected to strains higher than YS (elastic region), which generated active sites, thus improving the cathodic process, meaning that mass transport became the speed limiting step in the cathodic process.
- At the E_{corr} , all R_{ct} values are lower than the R_{ct} values obtained at any E_{cp} . This behavior indicates that the trend of the corrosion rate (CR) was affected by the applied cathodic potential, which prompted a decrease in CR; however, it is important to point out that the E_{cp} could improve the cathodic reaction, generating atomic H and increasing the susceptibility to SCC.

Author Contributions: Conceptualization, R.G.-M. and A.C.-H.; methodology, R.G.-M.; validation, R.G.-M., R.O.-C. and A.C.-H.; formal analysis, R.G.-M. and A.C.; investigation, R.O.-C. and E.M.-S.; resources, R.G.-M.; writing—original draft preparation, A.C. and R.G.-M.; writing—review and editing, R.O.-C. and M.A.M.-C.; visualization, E.M.-S.; supervision, R.G.-M. and A.C.; project administration, A.C.; funding acquisition, R.O.-C.

Funding: This research received no external funding.

Conflicts of Interest: The authors declare no conflict of interest.

References

1. Wang, L.W.; Du, C.W.; Liu, Z.Y.; Wang, X.H.; Li, X.G. Influence of carbon on stress corrosion cracking of high strength pipeline steel. *Corros. Sci.* **2013**, *76*, 486–493.
2. Torres-Islas, A.; Serna, S.; Campillo, B.; Colin, J.; Molina, A. Hydrogen embrittlement behavior on microalloyed pipeline steel in NS-4 solution. *Int. J. Electrochem. Sci.* **2013**, *8*, 7608–7624.
3. Cheng, Y. *Stress Corrosion Cracking of Pipelines*; John Wiley & Sons: Hoboken, NJ, USA, 2013.
4. Vasil'ev, V.Y.; Sergeeva, T.K.; Baldokhin, Y.V.; Ivanov, E.S.; Novosadov, V.V.; Bayankin, V.Y. Internal stresses, corrosion and electrochemical behavior in soils, and stress corrosion of pipe steels. *Prot. Met.* **2002**, *38*, 166–171.
5. Fang, B.Y.; Atrens, A.; Wang, J.Q.; Han, E.H.; Zhu, Z.Y.; Ke, W. Review of stress corrosion cracking of pipeline steels in “low” and “high” pH solutions. *J. Mater. Sci.* **2003**, *8*, 127–132.
6. Liang, P.; Li, X.; Du, C.; Chen, X. Stress corrosion cracking of X80 pipeline steel in simulated alkaline soil solution. *Mater. Des.* **2009**, *30*, 1712–1717.
7. Cui, Z.Y.; Liu, Z.Y.; Wang, L.W.; Ma, H.C.; Du, C.W.; Li, X.G.; Wang, X. Effect of pH value on the electrochemical and stress corrosion cracking behavior of X70 pipeline steel in the dilute bicarbonate solutions. *JMEP* **2015**, *24*, 4400–4408.
8. Cheng, Y.F. Thermodynamically modeling the interactions of hydrogen, stress and anodic dissolution at crack-tip during near-neutral pH SCC in pipelines. *J. Mater. Sci.* **2007**, *42*, 2701–2705.
9. Niu, L.; Cheng, Y.F. Corrosion behavior of X-70 pipe steel in near-neutral pH solution. *Appl. Surf. Sci.* **2007**, *253*, 8626–8631.
10. Tang, X.; Cheng, Y.F. Quantitative characterization by micro-electrochemical measurements of the synergism of hydrogen, stress and dissolution on near-neutral pH stress corrosion cracking of pipelines. *Corros. Sci.* **2011**, *53*, 2927–2933.
11. Liu, Z.Y.; Li, X.G.; Du, C.W.; Zhai, G.L.; Cheng, Y.F. Stress corrosion cracking behavior of X70 pipe steel in an acidic soil environment. *Corros. Sci.* **2008**, *50*, 2251–2257.
12. Fu, A.Q.; Cheng, Y.F. Electrochemical polarization behavior of X70 steel in thin carbonate/bicarbonate solution layers trapped under a disbonded coating and its implication on pipeline SCC. *Corros. Sci.* **2010**, *52*, 2511–2518.
13. Contreras, A.; Hernández, S.L.; Orozco-Cruz, R.; Galvan-Martínez, R. Mechanical and environmental effects on stress corrosion cracking of low carbon pipeline steel in a soil solution. *Mater. Des.* **2012**, *35*, 281–289.
14. Ohaeri, E.; Eduok, U.; Szpunar, J. Hydrogen related degradation in pipeline steel: A review. *Int. J. Hydrogen Energy* **2018**, *43*, 14584–14617.
15. Shahriari, A.; Shahrabi, T.; Oskuie, A.A. Effects of Cathodic Potential, Bicarbonate, and Chloride Ions on SCC of X70 Pipeline Steel. *JMEP* **2013**, *22*, 1421–1429.

16. Liu, Z.Y.; Li, X.G.; Cheng, Y.F. Mechanistic aspect of near-neutral pH stress corrosion cracking of pipelines under cathodic polarization. *Corros. Sci.* **2012**, *55*, 54–60.
17. NACE TM 0198. *Slow Strain Rate Test Method for Screening Corrosion-Resistant Alloys for Stress Corrosion Cracking in Sour Oilfield Service*; NACE International: Houston, TX, USA, 2016.
18. Zhang, G.A.; Cheng, Y.F. Micro-electrochemical characterization of corrosion of welded X70 pipeline steel in near-neutral pH solution. *Corros. Sci.* **2009**, *51*, 1714–1724.
19. McIntyre, D.R.; Kane, R.D.; Wilhelm, S.M. Slow strain rate testing for materials evaluation in high-pressure H₂S environments. *Corrosion* **1988**, *44*, 920–926.
20. Contreras, A.; Salazar, M.; Carmona, A.; Galván-Martínez, R. Electrochemical Noise for Detection of Stress Corrosion Cracking of Low Carbon Steel Exposed to Synthetic Soil Solution. *Mater. Res.* **2017**, *20*, 1201–1210.
21. Lynch, S.P.; Raja, V.S.; Shoji, T. Stress corrosion cracking: Theory and practice. Cambric mechanistic and fractographic aspects of stress-corrosion cracking (SCC). In *Stress Corrosion Cracking: Theory and Practice*; Raja, V.S., Shoji, T., Eds.; Woodhead Publishing: Cambridge, UK, 2011; pp. 1–88.
22. Liu, Z.Y.; Li, X.G.; Du, C.W.; Lu, L.; Zhang, Y.R.; Cheng, Y.F. Effect of inclusions on initiation of stress corrosion cracks in X70 pipeline steel in an acidic soil environment. *Corros. Sci.* **2009**, *51*, 895–900.
23. Martin, M.L.; Dadfarnia, M.; Nagao, A.; Wang, S.; Sofronis, P. Enumeration of the hydrogen-enhanced localized plasticity mechanism for hydrogen embrittlement in structural materials. *Acta Mater.* **2019**, *165*, 734–750.
24. Javidi, S.; Horeh, B. Investigating the mechanism of stress corrosion cracking in near-neutral and high pH environments for API 5L X52 steel. *Corros. Sci.* **2014**, *80*, 213–220.
25. Galván-Martínez, R.; Carmona, A.; Baltazar, M.; Contreras, A.; Orozco-Cruz, R. Stress Corrosion Cracking of X70 Pipeline Steel immersed in Synthetic Soil Solution. *Afinidad* **2018**, *76*, 52–62.
26. Marvasti, M.H. Crack Growth Behavior of Pipeline Steels in near Neutral pH Soil Environment. Master's Thesis, Department of Chemical and Materials Engineering, University of Alberta, Edmonton, AB, Canada, 2010.
27. Liu, Z.Y.; Lu, L.; Huang, Y.Z.; Du, C.W.; Li, X.G. Mechanistic aspect of non-steady electrochemical characteristic during stress corrosion cracking of an X70 pipeline steel in simulated underground water. *Corrosion* **2014**, *70*, 678–685.
28. Liu, Z.Y.; Li, X.G.; Du, C.W.; Cheng, Y.F. Local additional potential model for effect of strain rate on SCC of pipeline steel in an acidic soil solution. *Corros. Sci.* **2009**, *51*, 2863–2871.
29. Herraiz-Cardona, I.; Ortega, E.; Vázquez-Gómez, L.; Pérez-Herranz, V. Double-template fabrication of three-dimensional porous nickel electrodes for hydrogen evolution reaction. *Int. J. Hydrog. Energy* **2012**, *37*, 2147–2156.
30. Srinivasan, S. *Fuel Cells: From Fundamentals to Applications*; Springer Science & Business: New York, NY, USA, 2006.
31. Lebrini, M.; Lagrenée, M.; Vezin, H.; Traisnel, M.; Bentiss, F. Experimental and theoretical study for corrosion inhibition of mild steel in normal hydrochloric acid solution by some new macrocyclic polyether compounds. *Corros. Sci.* **2007**, *49*, 2254–2269.
32. Taylor, S.R.; Gileadi, E. Physical interpretation of the Warburg impedance. *Corrosion* **1995**, *51*, 664–671.
33. Bastidas, D.M. Interpretation of impedance data for porous electrodes and diffusion processes. *Corrosion* **2007**, *63*, 515–521.
34. Lasia, A. *Electrochemical Impedance Spectroscopy and its Applications*; Springer: New York, NY, USA, 2014.
35. Brug, G.J.; Van den Eeden, A.L.G.; Sluyters-Rehbach, M.; Sluyters, J.N.H. The analysis of electrode impedances complicated by the presence of a constant phase element. *J. Electroanal. Chem. Interfacial Electrochem.* **1984**, *176*, 275–295.
36. Liu, Z.Y.; Li, X.G.; Cheng, Y.F. Effect of strain rate on cathodic reaction during stress corrosion cracking of X70 pipeline steel in a near-neutral pH solution. *JMEP* **2011**, *20*, 1242–1246.

